Supplementary Material

1 QMAS ENCODING

Velocity compensated qMAS spherical tensor encoding (STE) (Lasič et al., 2014; Szczepankiewicz et al., 2015) was previously employed in combination with tuned and detuned linear tensor encoding (LTE), yielding large signal differences in fixed monkey brain tissue (Lundell et al., 2019a). The signal differences between tuned LTE and STE are related to microscopic anisotropy, while the differences between detuned LTE and tuned LTE are only due to time-dependent diffusion effects. The three encodings could thus in principle be used to correlate cell size and anisotropy. The results shown in the manuscript Figs. 9 and 12 include qMAS encoding waveforms shown here in Fig. S1.

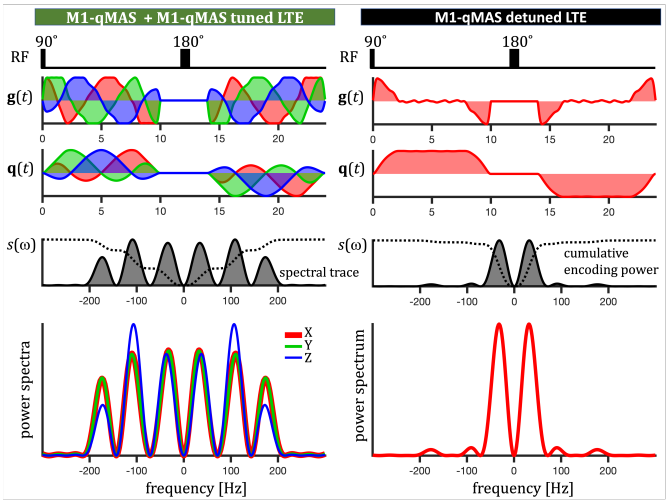

Figure S1. Radio frequency (RF) pulses, effective gradient waveforms $\mathbf{g}(t)$, dephasing waveforms $\mathbf{q}(t)$, normalized spectral trace $s(\omega)$ and diagonal components of the dephasing cross power spectral density (XYZ in red, green, blue) for M1-qMAS. The X component of qMAS was used as tuned LTE. Detuned LTE can be obtained from the magnitude of q-vector as described in (Lasič et al., 2014; Lundell et al., 2019a). Note the zero power at zero frequency characteristic of M1-encoding.

2 FITTING A SUBSET OF DATA FROM PIG HEARTS

The entire dataset, comprising mean diffusivity (MD) values from all encoding waveforms employed on the clinical scanner is shown in Fig. 7. In contrast, Fig. S2 features the results of fitting only MD values from a subset of data with long encoding times (τ = 67 ms), yielded comparable estimations of the two-compartment model parameters.

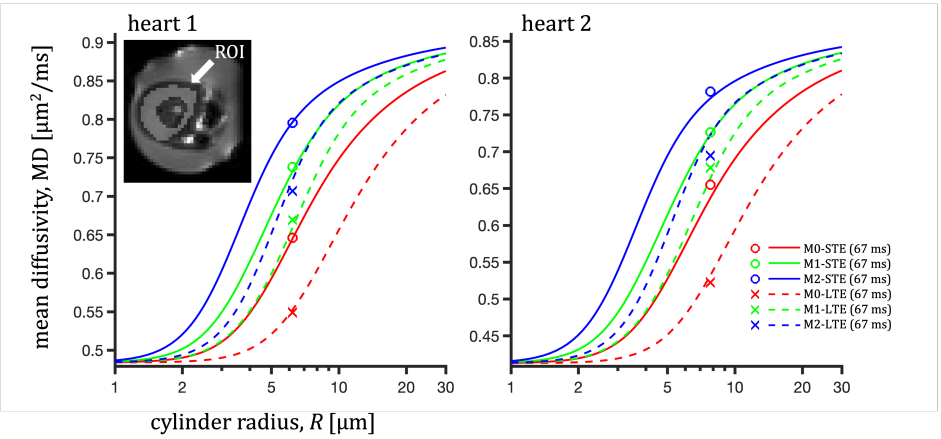

Figure S2. ROI-average mean diffusivity (markers) in the left ventricle myocardium in the central slice (short-axis view) of two pig hearts (left, right) and theoretical prediction (solid lines) from data at longer encoding times (τ = 67 ms).

3 EFFECTS OF BACKGROUND GRADIENTS

Szczepankiewicz and Sjölund proposed a ”cross-term sensitivity” metric for gauging the effects of background gradients (Szczepankiewicz et al. 2021), thus enabling optimization of free encoding waveforms for minimal or zero sensitivity to the adverse effects of background gradient *cross-terms*. The cross-term sensitivity for the preclinical waveforms is shown in Fig. S3

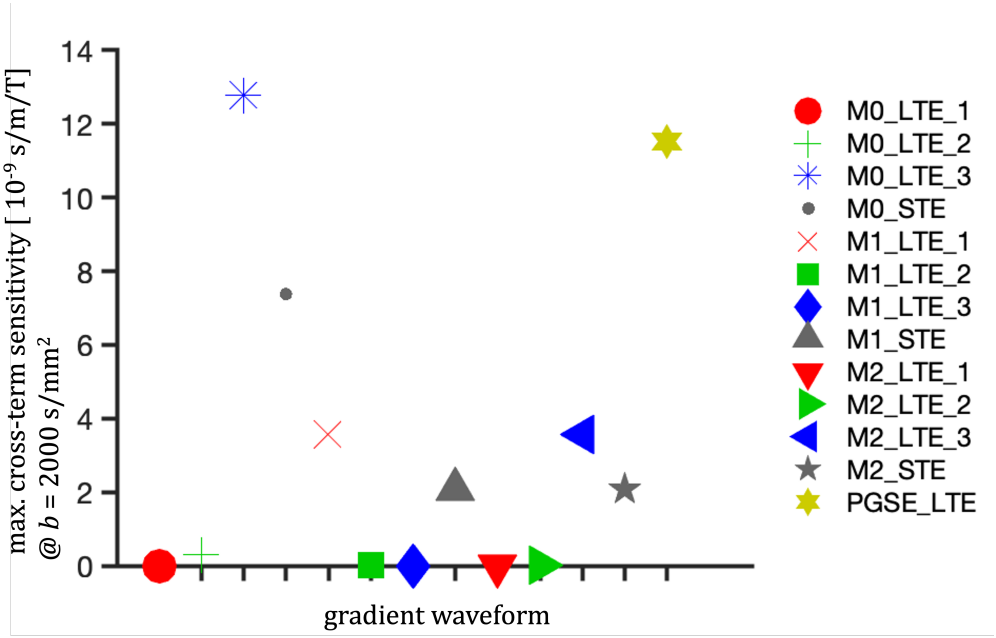

Figure S3. Cross-term sensitivity for various encoding waveforms. The maximum component of the cross-term sensitivity, as defined by Szczepankiewicz et al. 2021, is shown for each waveform assuming b-value of 2000 $\mathrm{s/mm^2}$.

Due to refocusing pulses in spin-echo sequences, a constant background gradient yields an additional time-dependent effective gradient,

$$\mathbf{g}_\mathrm{b}(t) = G_\mathrm{b}\,\mathbf{u}_\mathrm{b}\,h(t), \tag{S1}$$

where G_b and $\mathbf{u}_\mathrm{b}$ are background gradient's magnitude and direction (unit length), and $h(t)$ alternates between values of +1 and -1 in successive time intervals between the refocusing pulses.

This adds dephasing to the ”desired” (intended) effective gradient $\mathbf{g}_\mathrm{d}(t)$,

$$\mathbf{q}(t) = \mathbf{q}_\mathrm{d}(t) + G_\mathrm{b}\mathbf{u}_\mathrm{b}H(t), \tag{S2}$$

where

$$H(t) = \gamma \int_0^t h(t')dt'. \tag{S3}$$

Following the presented spectral-domain framework, i.e. considering attenuation to the first order in b, we can separate encoding spectra into three contributions (see also Eq. 3),

$$s_{ij}(\omega) = s_{ij}^{(\mathrm{d})}(\omega) + s_{ij}^{(\mathrm{c})}(\omega, G_\mathrm{b}\mathbf{u}_\mathrm{b}) + s_{ij}^{(\mathrm{b})}(\omega, G_\mathrm{b}\mathbf{u}_\mathrm{b}), \tag{S4}$$

where the first contribution is due to the desired dephasing (d), the third one is due to the background gradient (b) and the second contribution comprises mixed or "cross" terms between the desired and background dephasing (c). Note that a similar separation could be written for the spectral traces (Eq. 7). We emphasise that the last two terms depend on $G_\mathrm{b}\mathbf{u}_\mathrm{b}$. A similar expression can be found in Eqs. 15 and 16 in Szczepankiewicz et al. 2021 (cf. also Eq. 1 in Jara and Wehrli, 1994).

For simulation of multiple orientations of diffusion compartments and background gradients, it is important to consider how do the three terms in Eq. S4 scale. Since the first term scales as the b-value (trace), the second term as the product $\sqrt{b}G_\mathrm{b}$ and the last term scales as G_b^2, it is convenient to introduce the two corresponding unitless scaling factors, $\tilde{b}$ and $\tilde{G}_\mathrm{b}$, representing respectively the number of b-value units ($\mathrm{s/m^2}$) and the number of background gradient units ($\mathrm{T/m}$). We can thus rewrite Eq. S4 as

$$s_{ij}(\omega) = \tilde{b}\,\tilde{s}_{ij}^{(\mathrm{d})}(\omega) + \sqrt{\tilde{b}}\tilde{G}_\mathrm{b}\,\tilde{s}_{ij}^{(\mathrm{c})}(\omega, \mathbf{u}_\mathrm{b}) + \tilde{G}_\mathrm{b}^2\,\tilde{s}_{ij}^{(\mathrm{b})}(\omega, \mathbf{u}_\mathrm{b}). \tag{S5}$$

Here the rescaled encoding spectra, denoted with the tilde symbol, are calculated the same way as in Eq. S4 (see also Eq. 3) but using the appropriately scaled desired and background gradients. While the background gradient magnitude is set to G_b = 1 $\mathrm{T/m}$, the desired gradient amplitude is scaled such that

$$\frac{1}{2\pi}\int_{-\infty}^{\infty}\sum_{i=1}^{3}\tilde{s}_{ii}(\omega)d\omega = 1\,\mathrm{s/m^2}. \tag{S6}$$

By using the scaling factors we can thus factor out the dependence on b and G_b.

On scaling of cross-terms

It is interesting to consider how do the background gradient cross-terms scale and how they compare between clinical and preclinical systems. For general gradient waveforms with encoding time τ, excluding short gradient pulses, diffusion weighting due to cross-terms is proportional to $G_\mathrm{b}G_\mathrm{d}\tau^3$. Since the b-value scales as $G_\mathrm{d}^2\tau^3$, this leads also to scaling as $G_\mathrm{b}/G_\mathrm{d}\,b$ or as $G_\mathrm{b}\sqrt{b\tau^3}$.

Let us consider a three times stronger field and a ten times stronger G_d on a preclinical system compared to a clinical one. Assuming that background gradient magnitude scales linearly with the external field (Jara and Wehrli, 1994) and the same b-values are used on both systems, the above scaling would lead to 3 vs. 10 ratio of cross-term diffusion weighting on a preclinical vs. clinical system. The effect would be similar if 3 times higher b-values were used on a preclinical system. The relatively shorter encoding times, typically used on preclinical scanners, may thus be advantageous in keeping the effects of background gradients relatively low even at higher b-values.

Simulations of background gradient effects

Signals were calculated for preclinical gradient waveforms as outlined in the Methods section based on Eq. (2) for cylinders (averaged over 15 directions) and three sizes, but using the encoding spectra from Eq. S5, including the effects of background gradients applied along 50 evenly distributed directions. To account for potentially stronger background gradients on preclinical systems, we have used also higher G_b values of 3, 10 and 30 $\mathrm{mT/m}$ compared to 3 $\mathrm{mT/m}$ used in Szczepankiewicz et al. 2021. The result is shown in S4.

For reference we have included an example of two-compartment Gaussian diffusion, i.e. the intra voxel incoherent motion (IVIM) model as featured in Fig. 7 in Szczepankiewicz et al. 2021. We have used the

slow and fast diffusivities of D_s = 1 $\mu\mathrm{m}^2/\mathrm{ms}$ and D_f = 10 $\mu\mathrm{m}^2/\mathrm{ms}$, and the fraction of fast diffusing component of f_f = 0.1. In this calculation only the traces of $\tilde{s}_{ii}(\omega)$ were needed. The result is shown in S5.

We can see that the waveforms with low cross-term sensitivity (Fig. S3)) indeed exhibit low signal dispersion in Figs. S4 and S5. For the case of cylinders, differences between the rotation-averaged signals due to time-dependent anisotropic diffusion are still prominent in most settings. Importantly, these results suggest that background gradient effects are expected to be relatively small or negligible particularly for the M2 encoding used in our experiments. As expected, the effects are more pronounced for the waveforms with lower degree of motion compensation.

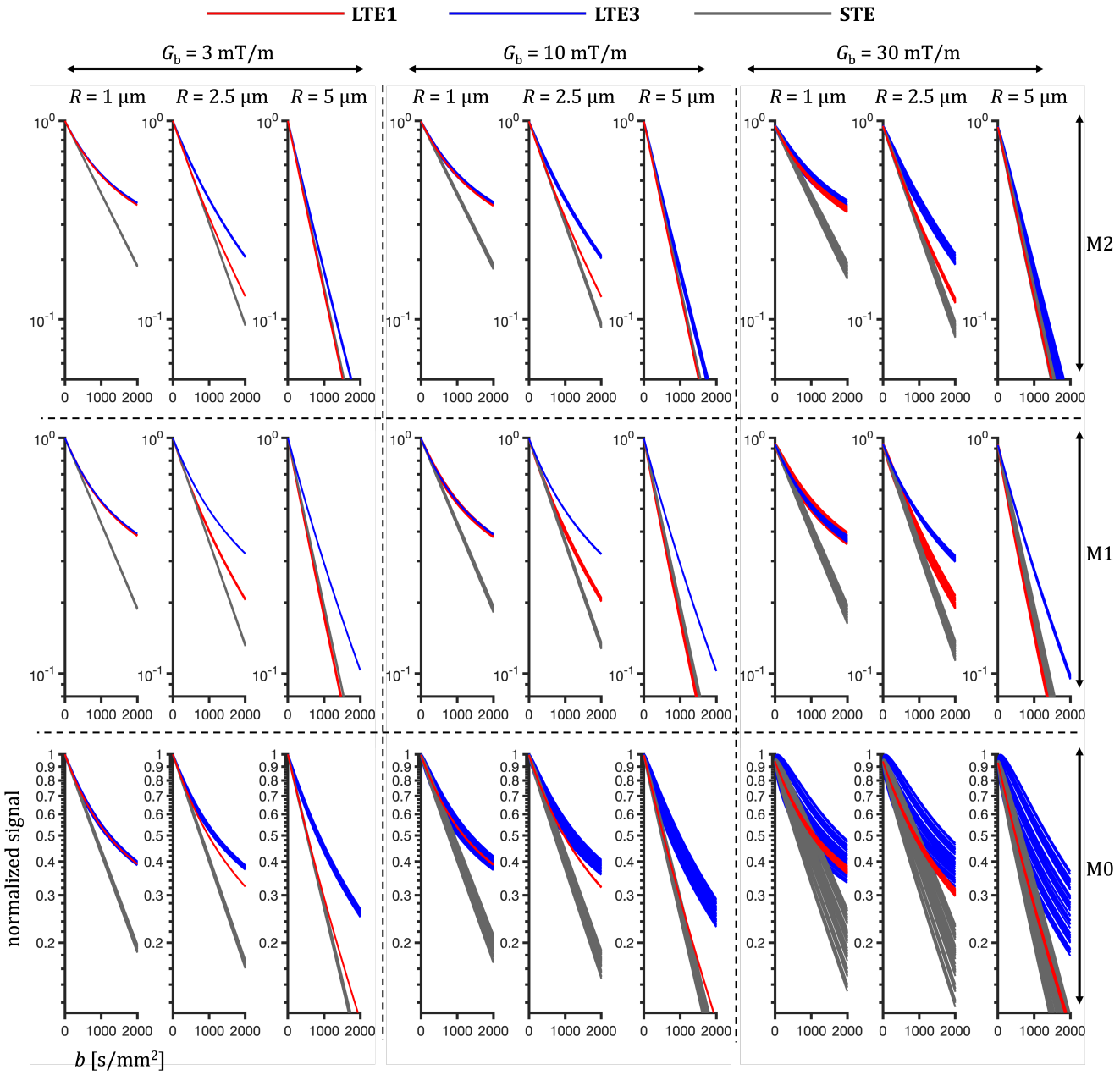

Figure S4. Simulated effects of background gradients on rotation-averaged signal from randomly oriented cylinders. Average signal vs. b-value was calculated for the preclinical waveforms (cf. Fig. 8) for 15 randomly oriented cylinders (D_0 = 2 $\mu m^2/ms$) and for 50 evenly distributed background gradient directions with varying amplitudes (G_b = 3, 10 and 30 mT/m). Outer columns from left to right show results for increasing G_b, while the inner columns are for increasing cylinder radii. The rows from bottom to top show results for increasing degree of motion compensation (M0-M2).

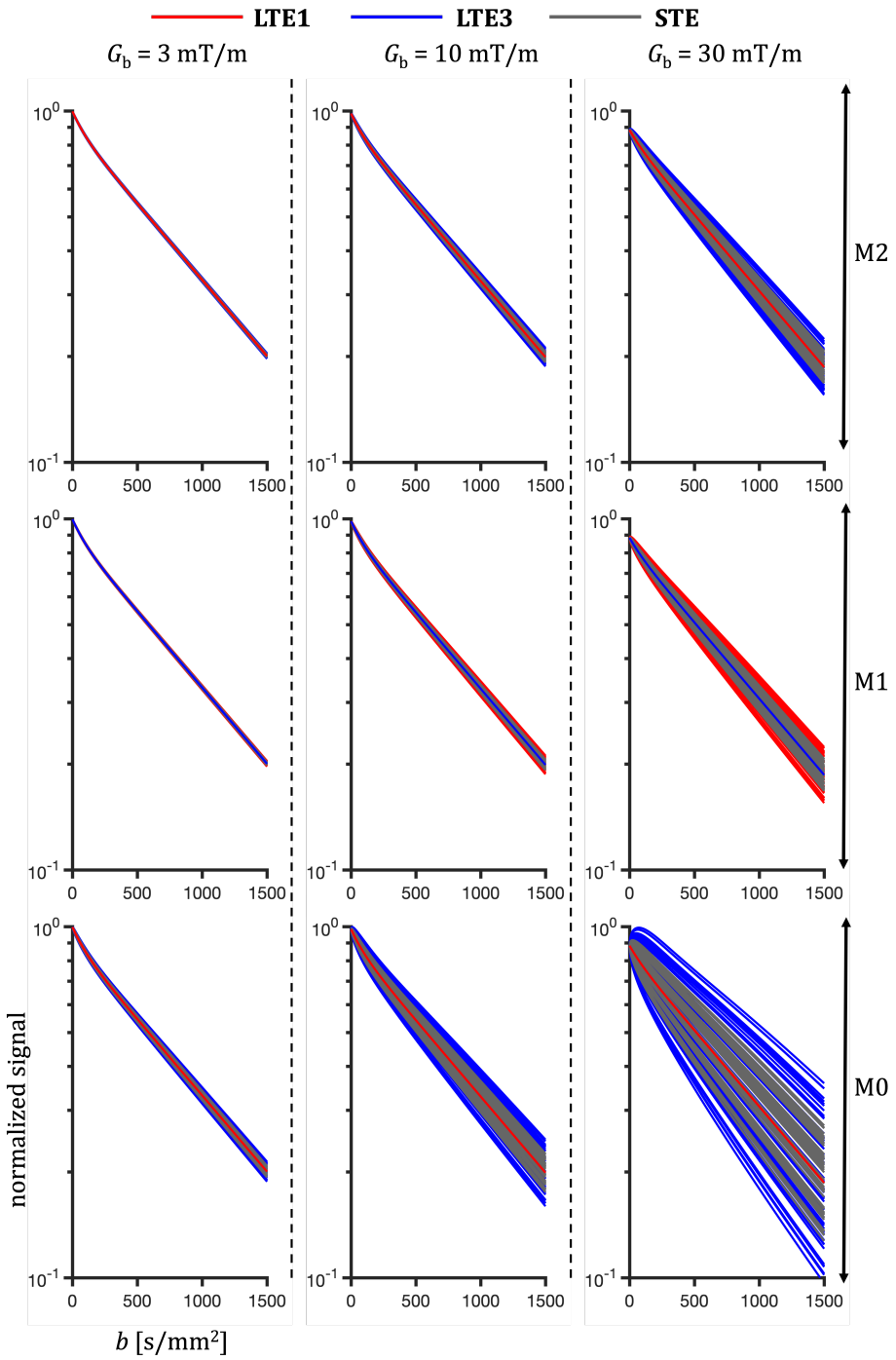

Figure S5. Simulated effects of background gradients on the IVIM signal. Signal vs. b-value was calculated as in Fig. S3, albeit no substrate averaging was needed in this case. Columns left to right show results for increasing G_b and rows from bottom to top show results for increasing degree of motion compensation (M0-M2).